Circulation Research

ORIGINAL RESEARCH

Glucose Derivative Induced Vasculopathy in Children on Chronic Peritoneal Dialysis

Maria Bartosova, Conghui Zhang, Betti Schaefer, Rebecca Herzog, David Ridinger, Ivan Damgov, Eszter Levai, Iva Marinovic, Christoph Eckert, Philipp Romero, Peter Sallay, Akos Ujszaszi, Markus Unterwurzacher, Anja Wagner, Georg Hildenbrand, Bradley A. Warady, Franz Schaefer, Sotirios G. Zarogiannis, Klaus Kratochwill*, Claus Peter Schmitt*

RATIONALE: Patients with chronic kidney disease (CKD) have an exceedingly high cardiovascular risk; which further increases in patients on peritoneal dialysis (PD). The pathophysiological role of reactive metabolites accumulating in CKD such as glucose degradation products (GDP) is uncertain.

OBJECTIVE: Delineating the impact of GDP present in PD fluids in accelerated vasculopathy development in patients with CKD.

METHODS AND RESULTS: Omental and parietal peritoneal tissues were obtained from 107 children with CKD before dialysis and 90 children on chronic PD with PD fluids containing very low or high concentrations of GDP. Omental arterioles, protected from local PD fluid exposure by surrounding fat, were microdissected for multiomics analyses. High-GDP exposed omental arterioles exhibited 3-fold higher advanced glycation endproduct concentrations and upregulated genes involved in cell death/apoptosis and suppressed genes related to cell viability/survival, cytoskeleton organization, and immune response biofunctions. Vasculopathy-associated canonical pathways concordantly regulated on gene and protein level with high-GDP exposure included cell death/proliferation, apoptosis, cytoskeleton organization, metabolism and detoxification, cell junction signaling, and immune response. Parietal peritoneal arterioles of patients exposed to high-GDP fluids exhibited lumen narrowing compared to patients with CKD stage 5 (end-stage kidney disease) and patients on low-GDP PD, intima thickness was increased. Protein quantification verified increased proapoptotic activity and cytoskeleton disintegration, single-molecule-localization microscopy demonstrated arteriolar endothelial ZO-1 (zonula occludens-1) disruption. Absolute and per endoluminal surface length, arteriolar endothelial cell counts inversely correlated with GDP exposure, caspase-3, TGF (transforming growth factor)-β–induced pSMAD2/3 (phosphorylated SMAD2/3), interleukin-6, ZO-1 abundance, and lumen narrowing. In vitro, 3,4-dideoxyglucosone-3-ene reduced lamin-A/C and membrane ZO-1 assembly, increased pSMAD2/3, and ionic and 4 and 10 kDa permeability of arterial endothelial cells.

CONCLUSIONS: Our findings indicate a fundamental role of GDP in PD-associated vasculopathy, exerted by endothelial cell junction and cytoskeleton disruption, and induction of apoptosis. They should redirect the focus of research and intervention on targeting reactive metabolite overload in CKD and PD.

REGISTRATION: URL: https://www.clinicaltrials.gov; Unique identifier: NCT01893710.

GRAPHIC ABSTRACT: An online graphic abstract is available for this article.

Key Words: apoptosis ■ chronic renal insufficiency ■ cytoskeleton ■ endothelium ■ peritoneal dialysis ■ proteome ■ vascular diseases

Editorial, see p 527 | In This Issue, see p 511 | Meet the First Author, see p 512

Correspondence to: Claus Peter Schmitt, MD, PhD, Division of Pediatric Nephrology, Center for Pediatric and Adolescent Medicine, Im Neuenheimer Feld 430, 69120 Heidelberg, Germany. Email clauspeter.schmitt@med.uni-heidelberg.de

*K. Kratochwill and C.P. Schmitt contributed equally.

The Data Supplement is available with this article at https://www.ahajournals.org/doi/suppl/10.1161/CIRCRESAHA.121.319310.

For Sources of Funding and Disclosures, see page e116.

Circulation Research is available at www.ahajournals.org/journal/res

Novelty and Significance

What Is Known?

- Chronic kidney disease is increasingly common and potentiates the cardiovascular risk, with a 40× higher risk in dialysis patients as compared to the age-matched general population.
- Peritoneal dialysis (PD) fluids contain various amounts of glucose degradation products (GDP), which are rapidly absorbed.

What New Information Does This Article Provide?

- In children on PD with high-GDP exposure, advanced glycation endproduct deposition is increased in omental arterioles protected from direct PD fluid exposure.
- Vascular disease–associated canonical pathways are concordantly regulated in arterioles on a gene and protein level with high-GDP exposure associated with cell death/proliferation, apoptosis, cytoskeleton organization, metabolism and detoxification, cell junction signaling, and immune response.
- Peritoneal arteriolar endothelial cell number is reduced with increased dialytic GDP exposure and arteriolar vessel lumen reduced due to intima thickening.

Patients on dialysis have an exceedingly high cardiovascular risk, the impact of reactive metabolites is debated. Conventional PD fluids contain high amounts of GDP, while GDP formation is largely prevented in costly double-chamber PD fluids. In omental arterioles from children with underlying diseases limited to kidney dysfunction and devoid of lifestyle factors, we demonstrate a 3-fold higher advanced glycation end product accumulation with high-GDP PD treatment. Multiomics analyses revealed activation of cell death and apoptosis pathways and suppression of cell viability/survival, cytoskeleton organization, and immune response biofunctions. In peritoneal arterioles endothelial number per endoluminal surface length is inversely related with GDP exposure, intima thickness is increased. Key protein quantifications verify increased proapoptotic activity and cytoskeleton disintegration; tissue single-molecule-localization microscopy demonstrates GDP-related reduced clustering of endothelial zona occludens-1 protein, which links the actin cytoskeleton to inter-endothelial junctions. In vitro studies reconfirm dose-dependent endothelial barrier disruption by GDP. Our findings challenge the use of PD fluids containing GDP and should redirect the focus of research on strategies to preserve endothelial integrity and barrier function in patients with dialysis-dependent chronic kidney disease.

Nonstandard Abbreviations and Acronyms

3,4-DGE	3,4-dideoxyglucosone-3-ene
AGE	advanced glycation end products
Casp3	caspase-3
CKD	chronic kidney disease
CKD5	CKD stage 5 (end-stage kidney disease)
CLDN1	claudin-1
GDP	glucose degradation products
IL	interleukin
L/V	lumen/vessel
p16	cyclin-dependent kinase inhibitor 2A
PD	peritoneal dialysis
PFN1	profilin 1
pSMAD2/3	phosphorylated SMAD2/3
RAGE	receptor for advanced glycation end products
ST2	suppressor of tumorigenicity 2
TGF	transforming growth factor
VEGF	vascular endothelial growth factor
ZO-1	zonula occludens-1

Cardiovascular disease is the leading cause of death worldwide.[1] Chronic kidney disease (CKD) is increasingly common due to the increasing prevalence of risk factors, such as obesity, hypertension, and diabetes mellitus and potentiates the cardiovascular risk. In dialysis patients, cardiovascular risk is particularly high, 40× higher than in the age-matched general population.[2] The role of reactive metabolites accumulating in CKD is uncertain.

The chronic administration of dialysis fluids in peritoneal dialysis (PD) patients provides a unique diagnostic window and research tool. Conventional PD fluids (PDF) contain high concentrations of glucose and high concentrations of glucose degradation products (GDP) generated during the heat sterilization process and prolonged storage. Following infusion into the peritoneal cavity, the acidic pH is rapidly equilibrated[3] and GDP are rapidly absorbed into the circulation and increase systemic concentrations of advanced glycation end products (AGE).[4,5] Separating glucose at a very low pH from the electrolytes and buffer compounds in double-chamber PD fluid bags largely prevents GDP formation and the associated systemic GDP load.[6–8] The impact of the PD-associated GDP load on cardiovascular health is unknown.

Most clinical trials failed to provide evidence for an improvement of relevant clinical outcomes, such as peritonitis incidence, PD technique outcome, cardiovascular health, and patient survival.[9]

Children are uniquely suited to study the pathophysiological mechanisms of vasculopathy since they are virtually devoid of aging and lifestyle-related factors, such as smoking, and the underlying diseases in the majority of cases are limited to the kidney and do not affect the vascular integrity. Studying omental arterioles is of particular interest because together with small arteries, they represent key segments of the vascular tree defining blood pressure.[10] Surrounded by fat tissue they are protected from immediate PD fluid–induced effects. Thus, these arterioles reflect vascular pathophysiology induced by CKD and by systemic PD–induced toxicity. Blood glucose concentrations remain in the physiological range in children on PD, disturbed glucose homeostasis, or diabetes mellitus are rarely observed.[11] The underlying pathomechanisms of systemic vasculopathy induced by CKD and PD-associated systemic toxicity have not yet been comprehensively assessed. We, therefore, analyzed omental arterioles and parietal peritoneal tissues obtained from pediatric patients with end-stage CKD either immediately before dialysis (CKD stage 5 [end-stage kidney disease; CKD5]) or after exposure to PD with fluids containing low and high concentrations of GDP by digital histomorphometry, transcriptomics, and proteomics. Key molecular findings were validated in the parietal peritoneal arterioles of matched patient subcohorts and in vitro.

METHODS

Data Availability

All materials and methods of this study are described in detail in the Data Supplement, please also see for Major Resources Table in the Data Supplement. Most relevant details are given here. The supporting data are available from the corresponding author upon request.

Study Population

The International Peritoneal Biobank comprises peritoneal tissue according to a standardized protocol from children at the time of Tenckhoff catheter insertion (CKD5) and on chronic PD. In patients on PD, the sampling site was at least 5 cm distant from the PD catheter entry site. Institutional review boards of the 27 participating centers approved the study. Written informed consent was obtained from parents and patients as appropriate. The study was performed according to the Declaration of Helsinki. None of the children selected were overweight (>85th height age-related body mass index percentile). After matching for age, glucose exposure, and PD duration, parietal peritoneal tissue of 60 double-chamber, low-GDP and 30 single chamber, high-GDP PD fluid–treated patients were selected and age-matched to 107 children with CKD5. Individual GDP exposure was calculated from the actual PD regime and GDP content of the administered PD, as published previously.[7,8] Treatment details are given in the Data Supplement.

Molecular mechanisms of vasculopathy were studied in omental arterioles in the CKD5, low-GDP PD, and high-GDP PD groups. Arterioles were microdissected from the surrounding fat tissue. mRNA and protein were isolated for transcriptome and proteome analysis (n=8 in CKD5, n=6 for high-GDP, and n=5 for low-GDP group). These children were matched for age, had noninflammatory underlying diseases, and no history of peritonitis, transplantation, or immunomodulatory therapy. PD patients were moreover matched for dialytic glucose exposure and PD duration.

For validation of the key molecular pathways identified by cross-omics in arterioles, parietal peritoneal tissue of 10 patients with low- and high-GDP PD fulfilling the same selection criteria as the omics cohort underwent digital immunohistochemistry analyses.

Transcriptome Analysis

Omental mRNA was isolated (RNAeasy; Qiagen, Hilden, Germany) and concentration and quality were determined. A total of 2.5 ng of mRNA with RNA integrity number >7 per sample were analyzed using Illumina Human Sentrix Beads microarray (Illumina, SanDiego) and scanned on iScan array scanner. Data import, extraction, background correction, normalization, and differential abundance analysis were done with R (http://www.r-project.org/) packages (illuminaHumanv4.db, beadarray, neqc, arrayWeights, and LIMMA). Raw data were submitted to ArrayExpress (http://www.ebi.ac.uk/arrayexpress) under the accession E-MTAB-9646.

Proteome Analysis

Protein concentrations and sample quality were assessed by SDS-PAGE. Filter-aided sample preparation and labeling of peptides with isobaric mass tags (TMT 11-plex, Thermo Fisher Scientific, Waltham, MA) were performed as described before.[12] Two-dimensional liquid chromatography was performed by reverse-phase chromatography at high and low pH. Mass spectrometry scans were performed on a QExactive (Thermo Fisher) liquid chromatography–mass spectrometry settings and raw data processing are described in detail in the Methods in the Data Supplement. Raw liquid chromatography–mass spectrometry data were submitted to PRIDE (Proteomics Identification Database) (https://www.ebi.ac.uk/pride/) under the accession PXD021747.

Pathway Analysis

Significantly regulated genes and proteins were submitted to analysis of enriched pathways, diseases, and biofunctions using the Ingenuity Pathway Analysis software (Qiagen, Hilden, Germany). Significantly enriched diseases and biofunctions with an activation Z score >1 or < −1 (cutoff $P<10^{-5}$ on the transcription level and cutoff $P<10^{-3}$ on the protein level) were extracted and clustered according to shared genes. Significantly enriched pathways were analyzed for associations

of the significantly regulated transcripts and proteins in vasculopathy. Vasculopathy-associated genes (n=2460) were extracted from Ingenuity Pathway Analysis and overlapped with significantly regulated transcripts and proteins. Pathways involved in vasculopathy were clustered according to shared genes. Pairwise similarity data (edges representing shared genes) were generated using R and visualized using Cytoscape 3.8.0 (www.cytoscape.org).

Tissue Immunohistochemistry

Histological stainings were performed according to standard methods. Parietal peritoneal arterioles of 60 to 100 µm diameter (5–7 per section) were analyzed. Stained sections at ≥5 different sites were analyzed for submesothelial thickness. Separate analyses of specific proteins in the mesothelial and submesothelial area did not reveal significant differences between the groups; therefore, total peritoneal data are given. For specific stainings, scanning, digital image analyses, and calculations, see expanded methods section.

Single-Molecule Localization Microscopy Data Analysis

The single-molecule localization microscopy microscope setup is described in expanded methods. The recorded single-molecule localization microscopy data were analyzed with in-house Python scripts, corresponding to MATLAB-based software described previously.[13,14] To reduce noise, a threshold of 3 was used and the first 30 frames of each stack were discarded.

The programs detect the position of the blinking dye molecules, use a 2-dimensional gaussian to calculate their position, and compile a matrix containing the signal amplitude, the *x*, *y* coordinates and the corresponding errors. Based on this matrix, relative distance distribution histograms (0–100 nm), signal-count boxplots, and pointillistic images of the vessels were created. The recorded images were manually sorted by blood vessel size to include only arterioles in the analysis.

For in vitro studies see extended methods.

Statistics

Descriptive data were summarized using proportions, means (SD), or medians (interquartile range). Normal distribution was assessed graphically and by Shapiro-Wilk test, Pearson, or Spearman correlations were calculated as appropriate.

T test or Mann-Whitney test were applied for testing of differences between 2 groups based on the data distribution. For describing differences in proportions, $\chi 2$ or Fischer exact test were used. Two-sided tests were applied unless stated otherwise. One-sided tests were used only in the validation cohort (n=10 per group) to confirm direction of regulation from comparison of 30 versus 60 patients for submesothelial thickness, microvessel density, blood vessel density, and lumen/vessel (L/V) ratio, which were significantly regulated. One-way parametric ANOVA as well as nonparametric Kruskal-Wallis was implemented for multiple group comparisons, with Holm-Sidak and Dunn methods, respectively, to adjust for multiplicity. For single-molecule localization microscopy cluster analysis and for ionic and solute permeability measurement, 2-way ANOVA followed by Holm-Sidak test was applied. GraphPad Prism 8 software (La Jolla) was used.

RESULTS

Omental Arteriolar Pathway Regulation With High-GDP Exposure

GDP-related systemic vascular effects were studied in omental arterioles microdissected from the surrounding fat from patients with CKD5 and on PD with low- and high-GDP fluids (Figure 1). Biochemical findings were not statistically different, as was the PD treatment in the PD groups (Table I in the Data Supplement). The arteriolar lumen/vessel (L/V) ratio was 0.58 (0.53–0.62) in CKD5, 0.59 (0.50–0.62) in patients with high-GDP, and 0.55 (0.50–0.61) in patients with low-GDP fluid exposure (P=0.72). Omental arteriolar AGE deposition was increased 3-fold with high compared with low-GDP exposure (12% [7.9–13.9] versus 1.5% [0.9–5.8] positive arteriolar area; P=0.043).

The arterioles underwent transcriptome and proteome analyses. Transcripts mapping to 11 920 genes as well as 3611 identified proteins (not counting proteins that were identified with only a single peptide) were quantified. Compared with CKD5, high-GDP exposure induced transcripts associated with 684 arteriolar genes and 137 proteins and suppressed 1560 genes and 55 proteins, whereas low-GDP exposure resulted in upregulation of only 145 transcripts and 110 proteins and downregulation of 38 transcripts and 34 proteins, respectively (raw P values, cutoff α=0.01; Figure I and Excel File I in the Data Supplement). Compared to CKD5, arteriolar exposure to low-GDP concentrations had a smaller effect (183/144 regulated transcripts/proteins) than high-GDP exposure (2244/192 regulated transcripts/proteins).

Directly comparing high- to low-GDP exposure yielded 2162 arteriolar transcripts (cutoff $P<0.01$, Figure 2A) associated with enriched activated diseases and biofunctions related mainly to cell death and apoptosis (66 functions with activation Z scores up to 10.4; cutoff $P<10^{-5}$) and deactivated functions related to organization of cytoskeleton, cell migration and cell survival and viability (155 functions; activation Z scores down to −8.0; Table II in the Data Supplement). Enriched functions (n=99) strongly activated or inactivated (Z score above 2.0 or below −2.0) were visualized according to shared genes, applying a minimum gene overlap of 20% for shown edges in the network (Figure 3A). On the protein level, the same cutoff of $P<0.01$ yielded 351 proteins (Figure 2B) with enriched activated diseases and biofunctions related to infection, lipid, and carbohydrate metabolism (75 functions; activation Z scores up to 3.9) and suppressed organismal survival and injury (31 functions; activation score down to −3.2).

The considerable overlap between the proteome and transcriptome, comprising 2713 unique gene names, confirmed the high quality of both experiments (Figure 2C). Protein coding genes not detected by

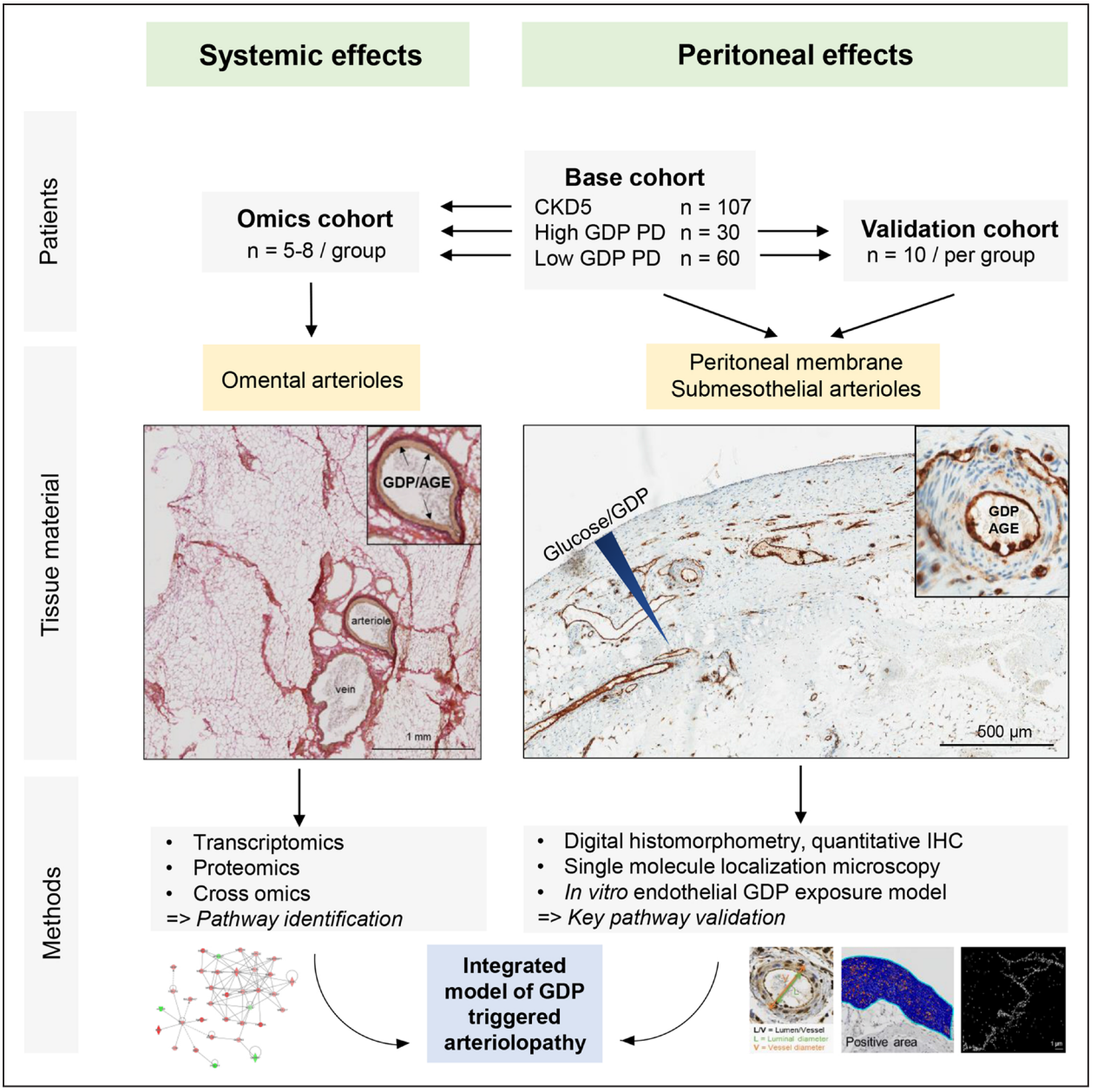

Figure 1. Overview on patient cohorts, tissues studied, and methods applied.
Omental arterioles from patients using peritoneal dialysis (PD) fluids with low–glucose degradation products (GDP) and high-GDP concentrations, respectively, were microdissected from the surrounding fat (preventing direct PD fluid exposure) and underwent multiomics analyses. Key findings were validated in submesothelial parietal peritoneal arterioles, exposed to GDP and high glucose concentrations. Methodologies and analytic approach are depicted in the **lower** parts. AGE indicates advanced glycation end products; CKD, chronic kidney disease; and IHC, immunohistochemistry.

the transcriptome analysis (n=846) were significantly enriched for membrane-associated lipoproteins, as well as for mitochondrial, nuclear body, and extracellular proteins. Transcripts not detected on the protein level (n=9206) were significantly more associated with low abundance genes, such as transcription factors, as well as intracellular and histone-associated genes (Excel File II in the Data Supplement).

Cross-omics analysis revealed 223 enriched (cutoff $P<0.01$) pathways on the transcriptomics or proteomics level (Excel File III in the Data Supplement). These were subsequently annotated with additional information on genes associated with vasculopathy in the Ingenuity Pathway Analysis knowledge base, clustered according to shared genes and visualized as a network (Figure 3B). Concordant differential regulation of vasculopathy-related canonical pathways associated with cytoskeleton organization, cell junction signaling, (glucose) metabolism and detoxification, cell death/proliferation and apoptosis, as well as immune response pathways.

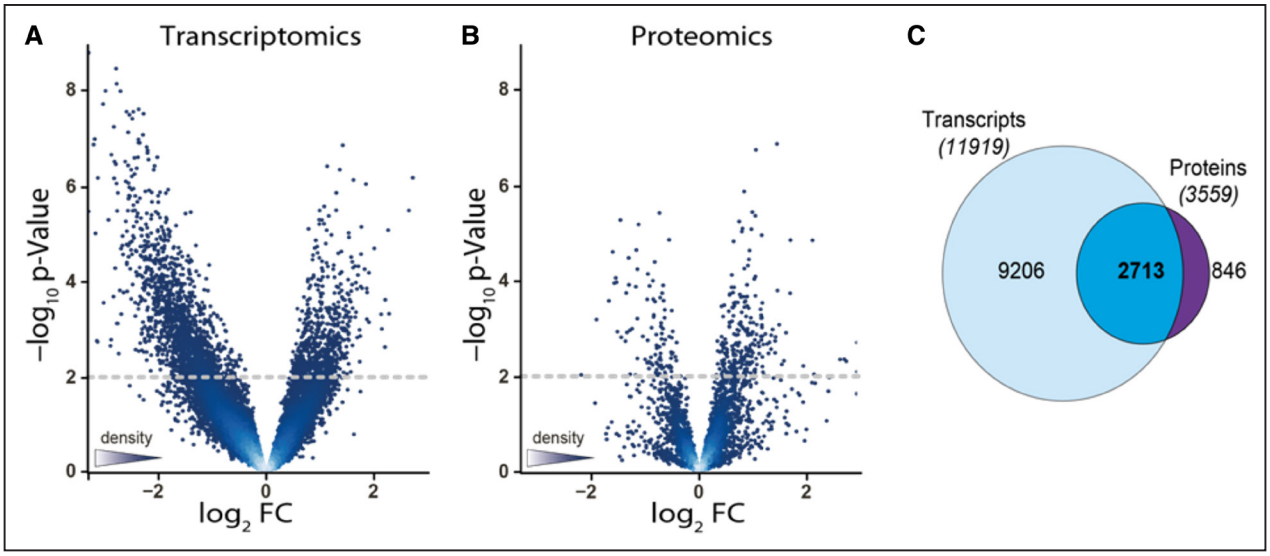

Figure 2. Regulation of omental arteriolar transcriptome and proteome.
Differentially regulated transcripts (**A**) and proteins (**B**) obtained from arterioles exposed to high–glucose degradation products (GDP; n=6) and low-GDP concentrations (n=5). **C**, Significant overlap in the identified proteins and genes. FC indicates fold change.

GDP Aggravates Parietal Peritoneal Vasculopathy and Fibrosis and Suppresses Angiogenesis

Parietal peritoneal tissues obtained from children with CKD5, low- and high-GDP PD, matched for age, PD duration, and dialytic glucose exposure, were analyzed by digital histomorphometry (Table III in the Data Supplement, Figure 1). Children treated with high-GDP fluid had developed more severe vasculopathy as indicated by a lower L/V ratio of parietal peritoneal arterioles and more pronounced submesothelial fibrotic thickening. Microvessel density was higher with low-GDP compared to high-GDP PD (Table 1). Lymphatic vessel density as quantified by podoplanin staining was 2-fold higher with high- versus low-GDP fluid exposure, diffuse podoplanin staining 3-fold more prevalent, generalizing a finding previously reported in patients with encapsulating peritoneal sclerosis.[15]

In multivariable analysis adjusting for PD fluid type, PD duration, glucose exposure, and the history of peritonitis, high-GDP PD usage was associated with increased vasculopathy and submesothelial fibrosis and lower microvessel density. The degree of submesothelial fibrosis also depended on the PD duration but to a much smaller extent than on GDP exposure (Table IV in the Data Supplement). Findings were gender independent.

Parietal Peritoneal Validation Studies

For quantitative cross-validation of omental arteriolar findings in parietal peritoneal arterioles, subgroups of children were selected applying the same rigorous criteria as for the arteriolar omics analysis. Biochemical findings were not statistically different, and daily total GDP exposure was 4× higher with high-GDP exposure (Table V in the Data Supplement). Histomorphometric findings of the primary cohort (Table 1) were reconfirmed. Vasculopathy was more severe with high-GDP exposure, ie, L/V ratio was lower, due to a higher intima thickness (Figure 4A), whereas media thickness and external vessel diameter were not statistically different between groups (Figure 4B, Table 2). Intima thickness correlated with GDP exposure (r=0.47, P=0.042). No vascular microcalcifications were detected. Submesothelial fibrosis was more pronounced, blood and lymphatic vessel density were reduced (Table 2), and inflammatory cell infiltration was lower with high-GDP PD.

GDP Induce Arteriolar Endothelial Apoptosis

Arteriolar omics analyses demonstrated marked activation of apoptosis pathways with high-GDP exposure (Figure 3). Similar to omental arterioles, AGE accumulation was higher in parietal peritoneal arterioles with high-GDP PD (P=0.062) and correlated to individual GDP and 3,4-dideoxyglucosone-3-ene (3,4-DGE) exposure (r=0.71/0.67, P=0.00032/0.0011; Table 3). The AGE receptor, RAGE, correlated with AGE abundance (r=0.38, P=0.078). Limiting the analysis to the arteriolar endothelium reconfirmed high-GDP exposure induced AGE deposition (P=0.0041), and Casp3 (caspase 3), p16 (cyclin-dependent kinase inhibitor 2A), and pSMAD2/3 upregulation (P=0.029, P=0.026, and P=0.020 compared with low-GDP exposure).

The structural protein of the nuclear envelope, lamin-A/C, was lower in omental arterioles on transcript and protein levels with high-GDP exposure and concordantly lower in peritoneal arterioles (Table 3, Figure 4C). Cleaved Casp3, a marker of apoptosis induction (Figure 4D), and

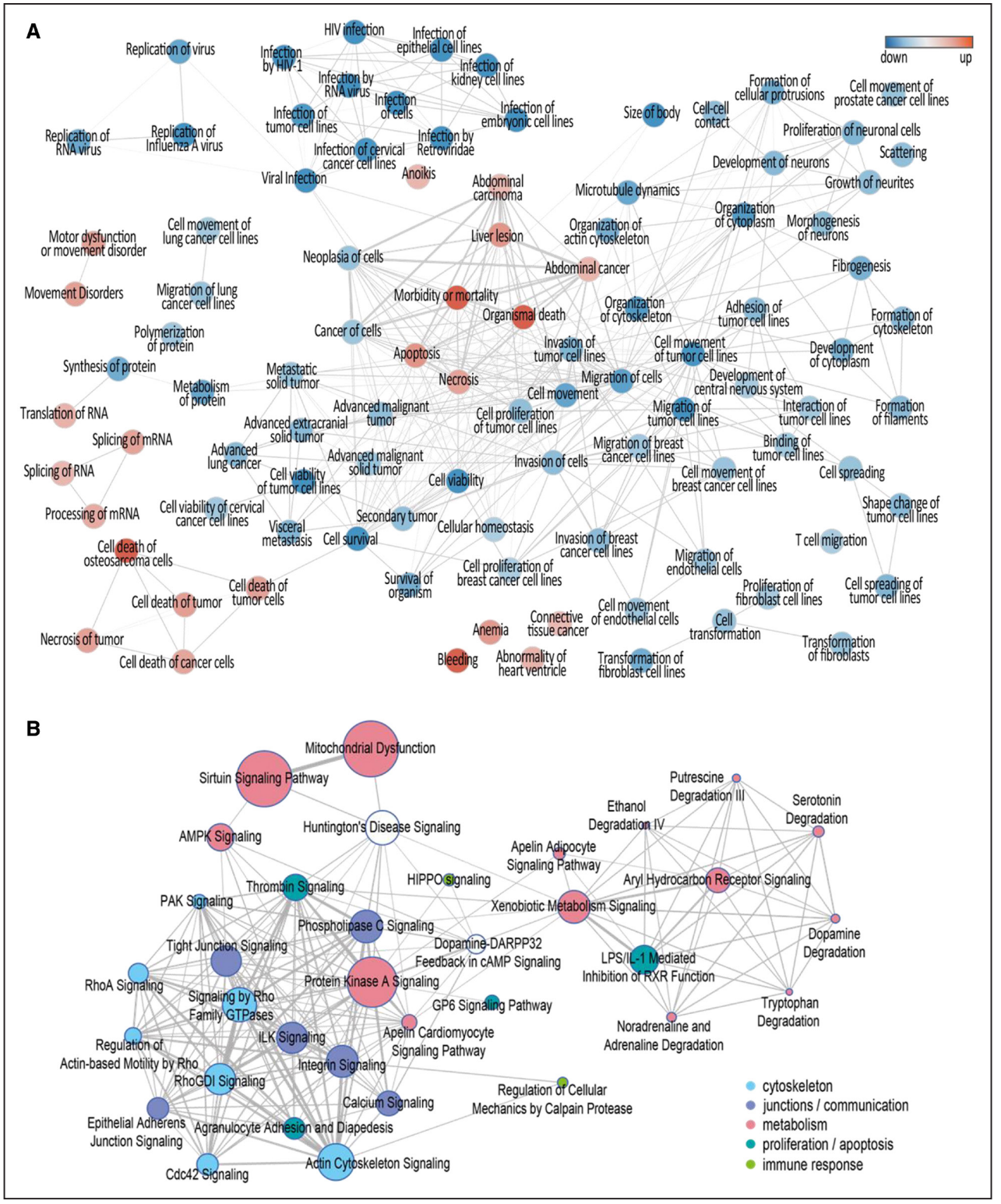

Figure 3. Network of enriched diseases and biofunction identified by transcriptomics and Network visualization of enriched vasculopathy-associated canonical pathways.

Network of diseases and biofunctions enriched in arterioles exposed to high–glucose degradation products (GDP) concentrations (n=6) as compared to arterioles exposed to low-GDP concentrations (n=5) are visualized according to shared genes, applying a minimum gene overlap of 20% for shown edges in the network. Ninety-nine strongly activated or inactivated (*Z* score above 2.0 or below −2.0) functions were included. Red circles indicate gene upregulation, and blue circles indicate downregulation (**A**). **B**, Respective enriched vasculopathy-associated canonical pathways (n=223) on transcriptomics or proteomics level annotated with information on vasculopathy-associated genes and clustered according to shared genes. AMPK indicates 5' adenosine monophosphate-activated protein kinase; DARPP32, dopamine- and cAMP-regulated neuronal phosphoprotein; ILK, integrin-linked kinase; LPS, lipopolysaccharide; PAK, p21-activated kinaseRhoGDI, Rho GDP-dissociation inhibitor; and RXR, retinoid X receptor.

Table 1. Histomorphometric findings of children with CKD5 and of children treated with high or low GDP PD.

	CKD5 (n=107)	High-GDP PD (n=30)	Low-GDP PD (n=60)	*P* value	*P* value (high vs low)
Age, y	8.6±6.0	8.54±5.3	8.3±5.7	0.97*	0.88*
Gender (male/female)	67/40	18/12	29/31	n.a.	n.a.
BMI	16 (15–18)	17 (15–20)	17 (16–18)	0.46†	0.93†
PD duration, mo	n.a.	18 (7–25)	14 (7–29)	n.a.	0.81†
Peritonitis [% patients with history of perit.]	n a.	28%	38%	n.a.	0.47‡
Glucose exposure, g (m^2·d)	n a.	86.0±50.1	94.2±33.7	n.a.	0.39*
Total GDP exposure, µmol/(d·m^2) BSA	n.a.	1490 (1078–1833)	138 (98–461)	n.a.	1.0×10^{15}†
3,4-DGE exposure, µmol (d·m^2) BSA	n.a.	72.6 (59.2–84.8)	5.8 (4.3–40.0)	n.a.	6.9×10^{9}†
L/V ratio	0.48±0.11	0.35±0.11	0.42±0.13	0.001*	0.016*
Mesothelial cell coverage (0–6)	4.1±1.7	2.6±2	2.2±2.1	7.4×10^{10}*	0.32*
Submesothelial thickness, µm	292±118	622±288	417±209	3.0×10^{15}*	13×10^{6}*
Total microvessel density, /mm^2	152±111	149±109	216±162	0.005*	0.021*
Sub. microvessel number, /mm	40±29	89±82	90±88	8.8×10^{7}*	0.960*
Diffuse podoplanin staining [% of pos. pat.]	0%	46%	18%	1.9×10^{10}‡	6.0×10^{3}‡
Lymphatic vessel density, /mm^2§	39±29	14±8	32±28	n.a.	n.a.‡§
Blood vessel density, /mm^2§	100 (49–153)	122 (36–245)	138 (67–253)	0.009†	0.13†
Blood vessel number, /mm§	24 (13–41)	36 (23–93)	52 (22–81)	5.7×10^{5}†	0.61†
Total endothelial surface area, µm^2/µm^3§	8.9 (5–15)	8.1 (5.2–17)	10.6 (6–18)	0.51†	0.46†
Lym. endothelial surface area, µm^2/µm^3§	2.4±2	2.0±1.4	2.9±2.6	n.a.	n.a.§
Blood vessel end. surface area, µm^2/µm^3§	7.3 (3–13)	6.9 (2–16)	8.2 (3–11)	0.75†	0.48†

3,4-DGE indicates 3,4-dideoxyglucosone-3-ene; BMI, body mass index; CKD5, chronic kidney disease stage 5 (end-stage kidney disease); GDP, glucose degradation product; L/V, lumen/vessel; n.a., not applicable; and perit., peritonitis.

*ANOVA was applied for comparison of the 3 groups and followed by post hoc comparison of high- vs low-GDP PD groups with Holm-Sidak correction for multiple testing. Student t test was used for parameters not applicable in patients with CKD5.

†Kruskal-Wallis test was used, followed by post hoc comparison of high- vs low-GDP PD group with Dunn correction for multiple testing. Mann-Whitney test was used for parameters not applicable in patients with CKD5.

‡Fisher exact test.

§Patients with diffuse podoplanin staining (precluding lymphatic vessel quantification) were excluded.

p16, a cell cycle arrest marker, were more abundant. Arteriolar AGE (r=0.62, P=0.0053), RAGE (r=0.55, P=0.014), Casp3, and p16 were correlated with IL (interleukin)-6 (r=0.40, r=0.71 and P=0.087, P=0.0011).

Both in absolute numbers and expressed relative to endoluminal surface length, the endothelial cell number was 40% and 23% lower in peritoneal arterioles from patients with high-GDP exposure. Also, endothelial circumference was lower (Table 2, Figure 4E), whereas the external arteriole diameter was not statistically different in both groups. The number of endothelial cells correlated with the L/V ratio (r=0.46, P=0.043), inversely with GDP exposure (r=–0.51, P=0.020, Figure 4F), AGE and RAGE (r=–0.41 and –0.71, P=0.072 and 0.0011), Casp3 (r=–0.48, P=0.038), IL-6 (r=–0.57, P=0.011), pSMAD2/3 (r=–0.49, P=0.054), ZO-1 (zonula occludens-1; r=–0.51, P=0.025), and p16 (r=–0.56, P=0.012). The relative endothelial cell number per µm endoluminal surface length correlated inversely with GDP exposure, with AGE, RAGE, IL-6, and p16 abundance (r=–0.51, r=–0.44, r=–0.68,r=–0.58, r=–0.54; P=0.025, P=0.056, P=0.0010, P=0.0093, P=0.016).

RAGE activation induces TGF (transforming growth factor)-β–SMAD signaling,[16] which is involved in the development of vasculopathy.[17,18] TGF-β downstream effector pSMAD2/3 was more abundant in parietal peritoneal arterioles with high-GDP exposure (P=0.06) and correlated with AGE/RAGE (r=0.62, P=0.0039/r=0.54, P=0.018), p16 (r=0.61, P=0.0062), and IL-6 abundance (r=0.68, P=0.0014, Table 3).

GDP-Induced Arteriolar Cytoskeleton and Tight Junction Disintegration

The arteriolar omics analysis demonstrated high-GDP exposure–related suppression of canonical actin cytoskeleton and tight junction pathways (Figure 4, Table II in the Data Supplement). Immunostaining demonstrated upregulation of the actin depolymerase Myo-1B (myosin1B) in peritoneal arterioles exposed to high-GDP, whereas no difference was observed for actin-binding protein profilin. ZO-1 connects intercellular junction proteins to the cytoskeleton and is involved in inflammation,[19] apoptosis,[20] and early vasculopathy.[21,22] Peritoneal arteriolar

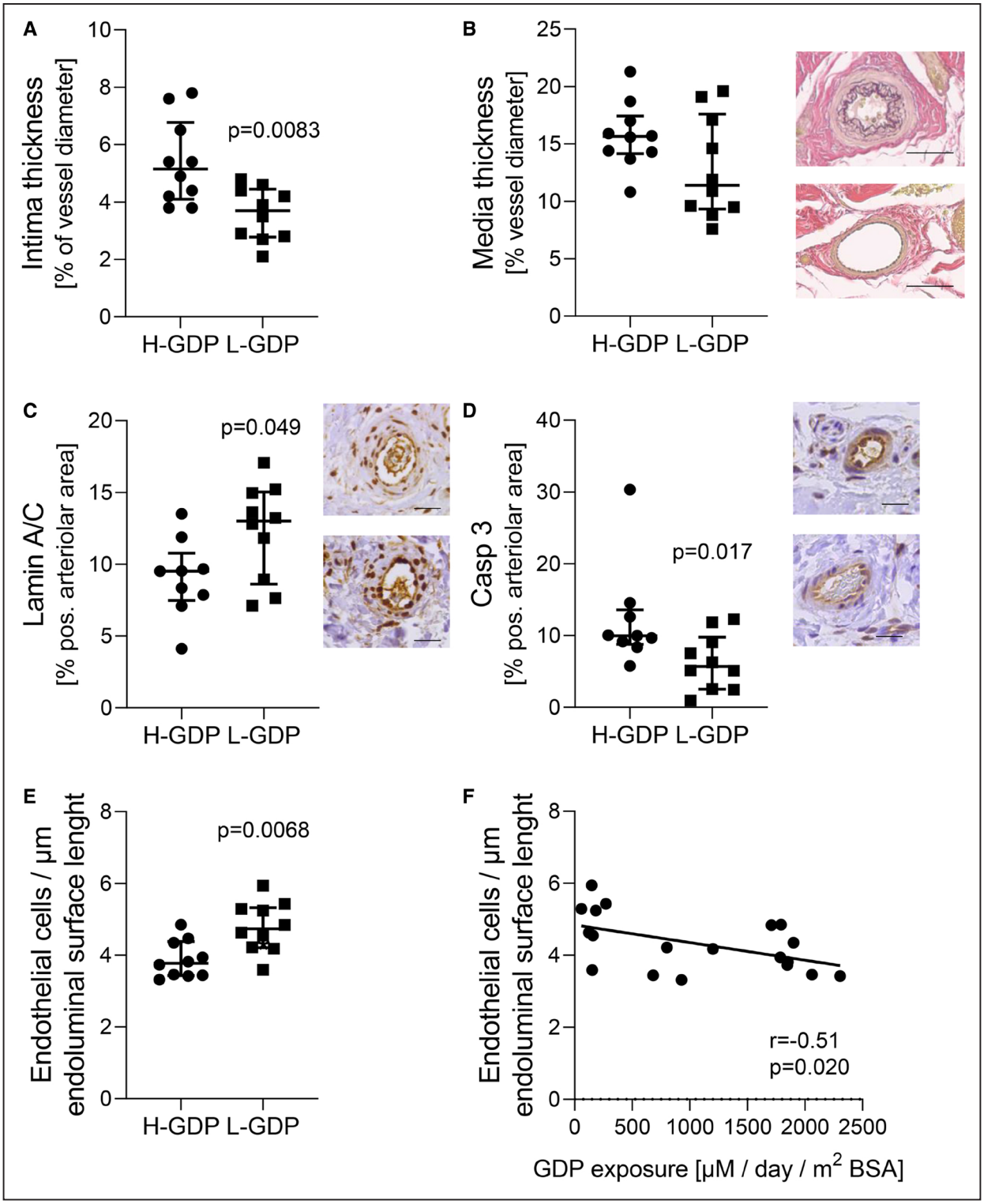

Figure 4. Arteriolar lumen narrowing and induction of arteriolar cell death pathways with high–glucose degradation products (H-GDP) peritoneal dialysis (PD).

Intima thickness is increased in patients with high-GDP exposure (**A**), media thickness (**B**) and external vessel diameter (see Table 2) are not statistically different. GDP/advanced glycation end product (AGE) induced apoptotic pathways in arterioles from H-GDP exposed patients. Lamin-A/C is suppressed (**C**) and Casp3 (caspase-3) induced (**D**) in parietal peritoneal arterioles from H-GDP patients, scale bars =50µm. Endothelial cell number per arterioles and per µm endoluminal surface length is reduced after H-GDP PD exposure (**E**) and (**F**) correlated with total GDP exposure (Spearman r=–0.51, P=0.020; **G**). n=10 per group, data are presented as median (interquartile range), Mann-Whitney test was applied in all comparisons. L-GDP indicates low-GDP; BSA, body surface area; and pos., positive.

Table 2. Peritoneal Morphology and Cellular Infiltration

	High-GDP PD (n=10)	Low-GDP PD (n=10)	*P* value
Age, y	2.8 (1.8–5.6)	4.9 (1.9–8.7)	0.35
Gender (male/female)	5/5	6/4	n.a.
BMI	17.4 (16.0–21.2)	16.9 (13.9–18.4)	0.46
PD duration, mo	18.5 (5.4–25)	11.5 (6.3–16.5)	0.45
Glucose exposure, g/(m²·d)	138 (101–159)	125 (94–147)	0.28
Total GDP exposure, µmol/(d·m²) BSA	1846 (1358–1982)	171 (143–900)	4.1×10^{4}*
3,4-DGE exposure, µmol (d·m²) BSA	70.9 (50.6–75.5)	7.0 (5.9–55.7)	0.027*
L/V ratio	0.45 (0.34–0.50)	0.52 (0.46–0.59)	0.042*
No. of endothelial cells per arteriole	6 (5.4–7.4)	9.3 (8.4–10.2)	6.9×10^{4}*
Endothelial cells/µm	3.8 (3.4–4.4)	4.7 (4.2–5.3)	6.8×10^{3}*
Endoluminal circumference, µm	166 (157–188)	188 (182–201)	0.018*
External vessel diameter, µm	80 (72–86)	77 (70–85)	0.68
Mesothelial cell coverage (0–6)	3.5 (0–4.3)	3.0 (1.5–6.0)	0.54
Submesothelial thickness, µm	680 (368–920)	480 (332–616)	0.050*
Total microvessel density, /mm²	53.0 (33–235)	246 (146–420)	0.012*
Blood vessel density, /mm²*	38 (27–228)	237 (124–366)	0.012*
Lymphatic vessel density, /mm²*	10 (6.3–16.7)	23 (14.5–47.1)	5.3×10^{3}*
Blood vessel end. surface area, µm²/µm³*	4.9 (3–13)	11.3 (10–20)	9.8×10^{2}*
Lym. endothelial surface area, µm²/µm³*	1.8 (1.3–4.9)	2.5 (1.2–4.1)	0.87
Lymphatic vessel perimeter, µm	146 (96–196)	99 (41–125)	0.023*
EMT [% pos. pat]	50%	10%	0.14†
ASMA positive [% patients]	20%	50%	0.34†
ASMA [/mm² in pos. patients]	60 (51–68)	29 (12–43)	0.092
CD45 positive [% patients]	50%	50%	0.99†
CD45 [/mm² in positive patients]	8 (4–9)	29 (20–51)	0.014*
CD68 positive [% patients]	50%	60%	0.99†
CD68 [/mm² in positive patients]	8 (5–15)	25 (19–46)	0.021*
Mast cells [cells/mm²]	14 (13–17)	22 (14–33)	0.025*
Tryptase release/mast cell [pixel]	5829 (4396–8096)	12556 (5090–13510)	0.043*

Mann-Whitney test was used unless indicated by

†. 3,4-DGE indicates 3,4-dideoxyglucosone-3-ene; ASMA, alpha smooth muscle actin; BMI, body mass index; EMT, epithelial-mesenchymal transition; GDP, glucose degradation product; L/V, lumen/vessel; lym., lymphatic; n.a., not applicable; pat., patient; PD, peritoneal dialysis; and pos, positive.

*In each group, 1 patient with diffuse podoplanin staining was excluded from respective analysis.

†Fisher exact test was used.

ZO-1 abundance did not differ between the high- and low-GDP groups (Table 3) but correlated with the L/V ratio (r=–0.52, P=0.021), Casp3 (r=0.43, P=0.061), p16 (r=0.54, P=0.016), and IL-6 (r=0.50, P=0.028).

Because endothelial integrity depends on the spatial organization of the intercellular junctions, we performed single-molecule localization microscopy of ZO-1. The spatial organization of the arteriolar endothelial ZO-1 molecules was analyzed according to Ripley distance frequency curve shapes. Peaks occurring in these curves indicate molecular cluster formation, a signature correlated to functionality of membrane-embedded molecules.[23] The slope of the Ripley curves at higher distances reflect the degree of randomness of the surrounding points.[18] The degree of ZO-1 clustering in arteriolar endothelial cells was lower with high-GDP PD, suggesting less densely organized ZO-1 molecules in the junctional area (Figure 6A), the degree of randomness of the surrounding points was much higher. Most frequent distances between single ZO-1 molecules were higher with high-GDP compared with low-GDP exposure (92 [54.5–97] nm versus 34.5 [28.3–42] nm; P=6.1×10^{-9}, Figure 6B). No difference was observed for the number of membrane-bound ZO-1 molecules per nm² ([4.33±3.10] 10^{-6} and [4.68±3.65] 10^{-6} counts/nm², P=0.70; Figure 6C). Sealing junction CLDN1 (claudin-1) abundance in parietal arterioles was not statistically different between the groups but in arterioles with high-GDP exposure, correlated with L/V ratio (r=0.63, P=0.061), that is, inversely with vasculopathy.

Table 3. Parietal Arteriolar Protein Regulation

	High-GDP PD (n=10)	Low-GDP PD (n=10)	*P* value (Mann-Whitney test)
AGE [% pos. area]	9.4 (6.9–15.1)	5.5 (3.2–8.8)	0.062
RAGE [% pos. area]	17.6 (9.3–27.6)	8.8 (5.4–18.1)	0.11
Lamin-A/C [% pos. area]	9.5 (7.5–10.7)	13.0 (8.6–15.0)	0.049
Casp3 [% pos. area]	10.0 (8.8–13.6)	5.6 (2.5–9.7)	0.017
p16 [% pos. area]	14.0 (8.5–31.8)	8.3 (2.7–16.4)	0.065
IL-33 [% pos. area]	7.5 (6.8–9.9)	6.3 (4.7–11.5)	0.19
ST2 [% pos. area]	29.4 (22.1–35.1)	20.9 (18.6–28.0)	0.13
pSMAD2/3 [% pos. area]	15.7 (11.1–25.2)	11.2 (5.9–17.3)	0.062
IL-6 [% pos. area]	21.9 (13.3–30.4)	11.2 (3.9–19.5)	0.068
Ki67 [% pos. area]	3.6 (1.8–7.1)	2.5 (0.6–8.4)	0.51
VEGF-A [% pos. area]	5.9 (3.3–7.3)	6.1 (4.5–10.1)	0.59
Myo-1B [% pos. area]	14.7 (8.6–20.5)	7.7 (4.6–11.7)	0.018
PFN1 [% pos. area]	9.6 (5.6–11.3)	10.3 (6.0–13.5)	0.59
ZO-1 [% pos. area]	44.8 (39.4–51.8)	37.8 (35.3–44.5)	0.16
CLDN1 [% pos. area]	6.7 (5.4–9.1)	7.4 (4.4–9.4)	0.68

AGE indicates advanced glycation end products; Casp3, caspase-3; CLDN, claudin-1; GDP, glucose degradation product; IL, interleukin; Myo1B, myosin1B; PD, peritoneal dialysis; PFN1, profilin 1; pos., positive; pSMAD, phosphorylated SMAD; RAGE, receptor for advanced glycation end products; ST2, suppressor of tumorigenicity 2; VEGF, vascular endothelial growth factor; and ZO-1, zonula occludens-1.

High-GDP Exposure Inhibits Submesothelial Angiogenesis and Immune Response and Enhances Fibrosis

GDP exposure was associated with suppression of omental arteriolar genes involved in endothelial cell migration/movement (Table II in the Data Supplement), Ingenuity Pathway Analysis demonstrated downregulation of the angiogenesis pathway (activation *Z* score –0.8, $P=5.0\times10^{-5}$). In line with this, parietal peritoneal vessel density was lower with high-GDP PD as compared to low-GDP PD. Peritoneal VEGF (vascular endothelial growth factor)-A was 50% lower with high-GDP than with low-GDP PD (Table VI in the Data Supplement), and correlated negatively with the individual GDP and 3,4-DGE exposure ($r=-0.51$, $P=0.024$ and $r=-0.45$, $P=0.051$) and with microvessel density ($r=0.44$, $P=0.050$). IL-17 abundance, a recently proposed mediator of peritoneal angiogenesis via VEGF,[24] was 3.8-fold lower with high-GDP PD and correlated with the GDP and 3,4-DGE exposure ($r=-0.54$, $P=0.021$ and $r=-0.43$, $P=0.073$), with microvessel density ($r=0.46$, $P=0.043$) and in the low-GDP group with VEGF-A abundance ($r=0.66$, $P=0.031$).

Omental arteriolar GDP exposure also downregulated immune cell trafficking and cell-mediated immune response (Table II in the Data Supplement). In line with this, peritoneal immune cell infiltration was low with high-GDP PD, that is, few CD45 leukocytes, CD68 macrophages, and mast cells were present; tryptase release per mast cell was lower compared with low-GDP PD (Table 2). Total submesothelial tryptase inversely correlated with GDP exposure ($r=-0.47$, $P=0.032$) and with VEGF-A abundance ($r=0.39$, $P=0.089$).

IL-33, which has been suggested to exert tissue-protective and antifibrotic actions,[25] and IL-6 inversely correlated with the increased submesothelial thickness ($r=-0.84$, $P=0.011$; $r=-0.75$, $P=0.0044$) but not with inflammatory cell infiltration. IL-33 receptor ST2 (suppressor of tumorigenicity 2) was not statistically different. EMT (epithelial-mesenchymal transition) cells, a key component of submesothelial fibrosis development,[26] were detected in 5 out of the 10 patients in the high- and 1 out of 10 patients in the low-GDP group (Table 2).

In Vitro Validation of Key Arteriolar Findings

Human umbilical arterial endothelial cells were treated for 24 hours with increasing doses of 3,4-DGE as present in high-GDP PD fluids. 3,4-DGE dose-dependently reduced perinuclear lamin-A/C. Similar findings were obtained for human umbilical vein endothelial cells treated for 24 hours and for 5 hours per day over 3 and 7 consecutive days with increasing doses of 3,4-DGE (Figure II in the Data Supplement). In the same direction, increasing doses of 3,4-DGE resulted in upregulation of pSMAD2/3 and a progressive disruption of membrane ZO-1. Respective functional studies demonstrated a dose-dependent decline in transendothelial electrical resistance and increased permeability for 4 kDa dextran with 5 to 20 µmol/L of 3,4-DGE exposure (Figure 6).

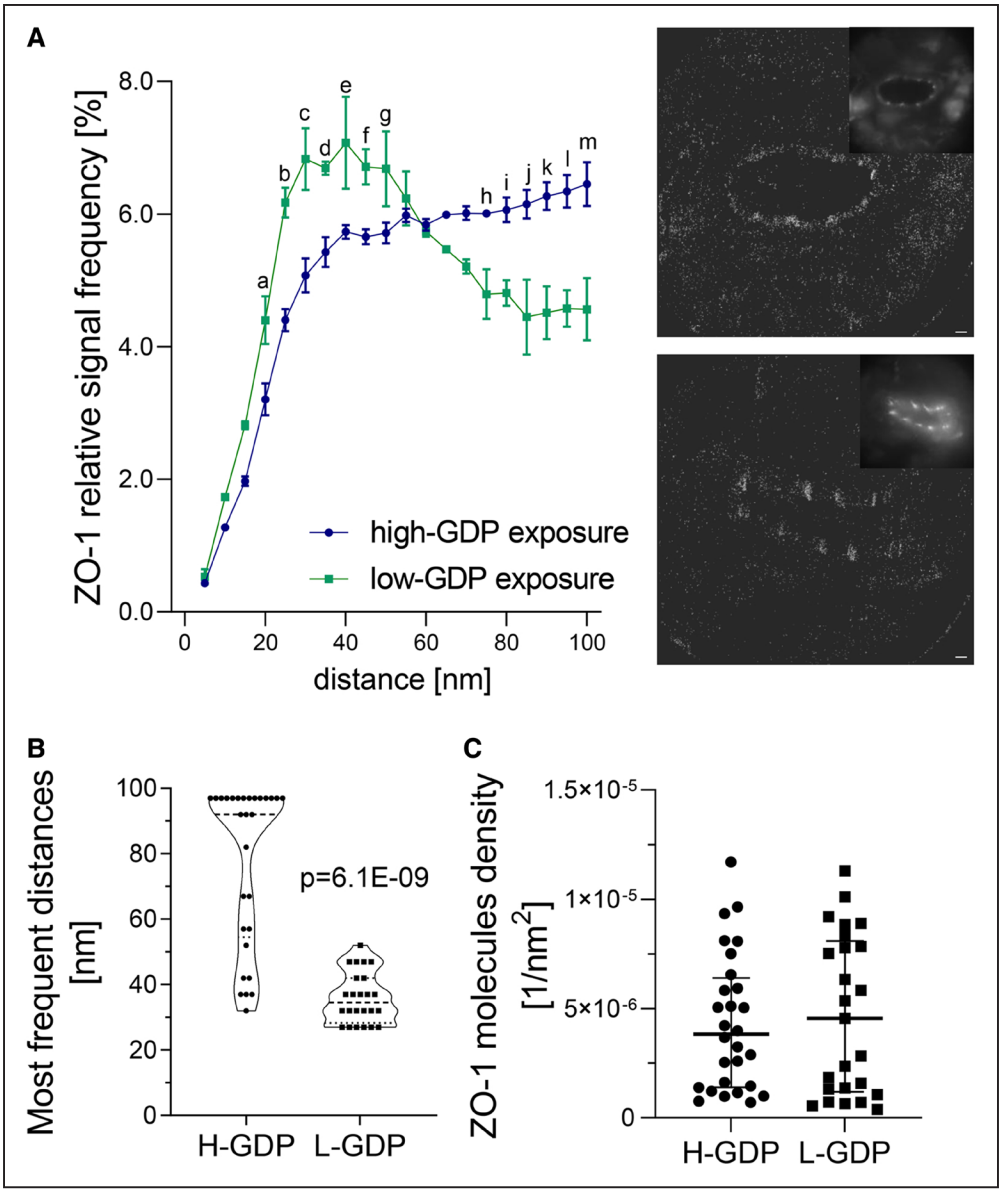

Figure 5. Endothelial ZO-1 (zonula occludens-1) clustering is modified by high–glucose degradation products (H-GDP) peritoneal dialysis (PD).

A, Single-molecule localization microscopy quantification of ZO-1 clustering within 100 nm distance in parietal peritoneal arteriolar tissue sections of low-GDP (L-GDP)–treated and H-GDP–treated patients (n=3 per group). The representative images on the right give an overview of single arterioles (inset in the **upper right** corners) and single ZO-1 molecule visualization with H- (**upper** image) and L-GDP PD (**lower** image), scale bar=10 µm. Data are presented as median (interquartile range [IQR]), 2-way ANOVA followed by Holm-Sidak test for multiple comparison was applied. Letters indicate significant differences between the groups, individual *P* values are listed in Table VII in the Data Supplement. **B**, The respective frequencies of the distances between single ZO-1 molecules, (**C**) the membrane-bound ZO-1 molecules per nm^2, n=25. In **B** and **C**, data are presented as median (IQR), Mann-Whitney test was applied.

DISCUSSION

Reactive metabolites play a key role in the aging process and aging-related disorders including neurodegenerative and psychiatric diseases.[27,28] Long-term complications of diabetes mellitus are driven by reactive glucose metabolites.[29,30] Reactive metabolites also accumulate in patients with CKD and normal glucose homeostasis; their impact on patient outcome, however, is uncertain.[31] With regards to the peritoneal dialysis treatment modality, it is still controversial whether the high concentrations of reactive metabolites present in conventional PD fluids, such as the highly reactive dicarbonyl compounds methylglyoxal and 3,4-DGE, impact PD patient outcome. High-GDP PD fluids are still widely used since improved outcomes with the use of low-GDP fluids have not been demonstrated to date.[9,32] Here, we provide evidence that GDP play a fundamental role in arteriolar remodeling.

PD fluids exert metabolic tissue stress, which declines with penetration depth.[33] The omental arterioles analyzed

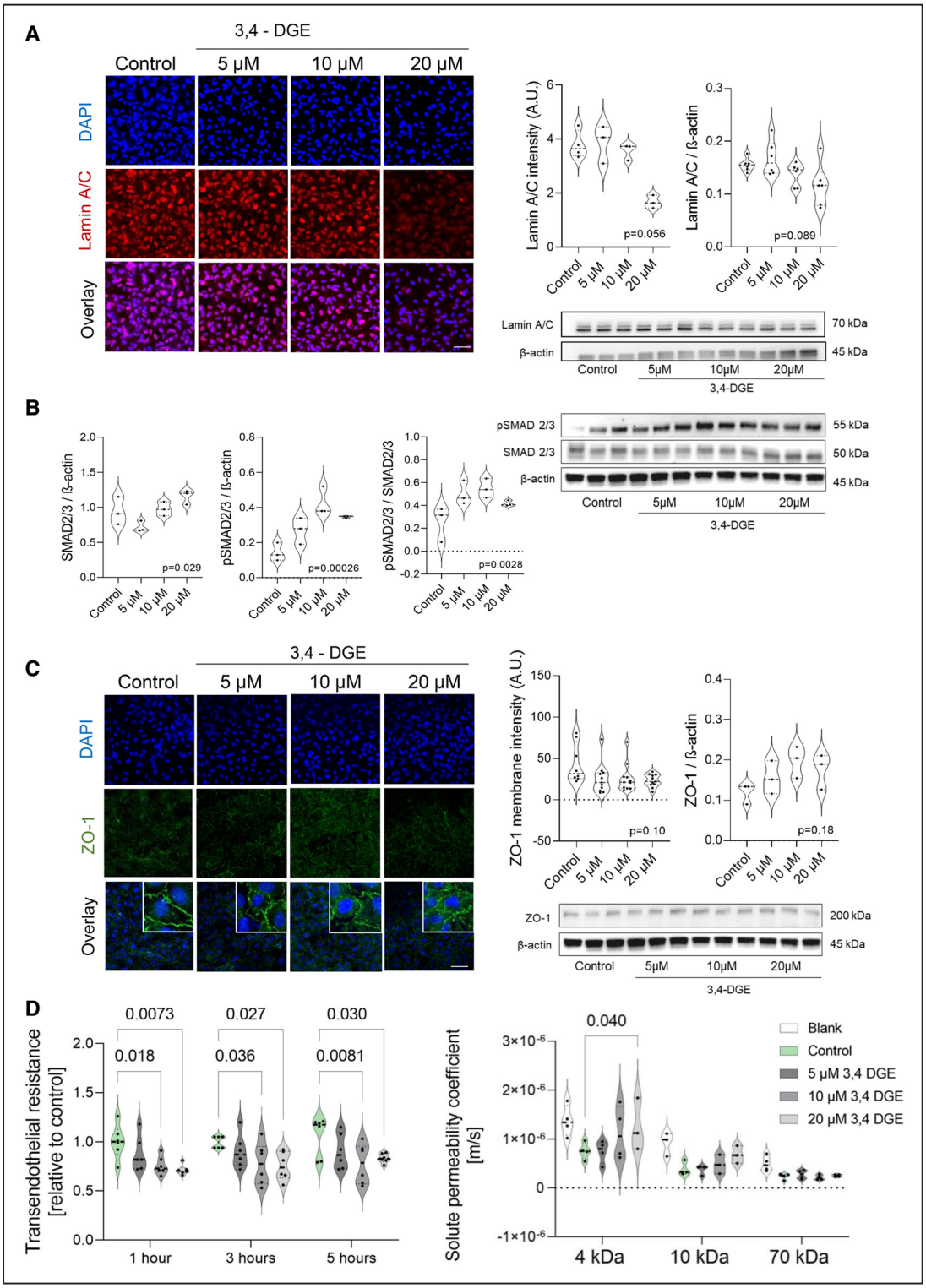

Figure 6. 3,4-dideoxyglucosone-3-ene (3,4-DGE) suppresses lamin-A/C, induces phosphorylation of SMAD2/3, disrupts membrane ZO-1 (zonula occludens-1), and increases endothelial monolayer permeability.
Human umbilical arterial endothelial cells (HUAEC) were treated with 3,4-DGE at concentrations as present in high–glucose degradation products (GDP) fluids for 24 h. **A**, 3,4-DGE dose-dependently decreases lamin-A/C. A representative IF staining is given on the **left** side, Image-J quantification in the **middle** (n=3), a representative WB on the **lower right**, and respective quantification of the WB on the **upper right** (n=6). **B**, Phosphorylation of SMAD2/3 is increased (n=3). **C**, Total endothelial ZO-1 is unchanged (n=3), cell membrane ZO-1 is disintegrated (n=10). **A**–**C**, Analyzed by nonparametric Kruskal-Wallis test). Scale bars=50 µm. **D**, In transwells, HUAEC paracellular ionic permeability (transendothelial electric resistance, presented as relative change to medium control, n=6), and 4, 10, and 70 kDa dextran permeabilities in response to increasing concentrations of 3,4-DGE are given (n=6), 2-way ANOVA followed by comparison of treatment vs control group with Holm-Sidak correction was applied. A.U. indicates arbitrary units; DAPI, 4′,6-Diamidin-2-phenylindol; IF, immunofluorescence; pSMAD, phosphorylated SMAD; and WB, western blot.

in our study were surrounded by at least 1 mm of fat tissue and should reflect systemic effects of the PD fluids, that is, the specific effects of absorbed GDP. 90% of the osmotic gradient exerted by PD fluids dissipates within the superficial 400 µm of the peritoneal membrane.[33] They were carefully selected from young pediatric patients, devoid of confounding lifestyle-related factors and with underlying diseases not affecting vascular integrity. Within the 3 cohorts studied, there were no statistical differences in anthropometric and biochemical findings and regarding the PD prescriptions in the 2 PD cohorts, except for the PD-associated GDP load. Thus, despite the limited number of patients with high-GDP fluid usage available for analysis a highly sensitive analysis could be accomplished. Our cross-omics approach leverages specific advantages of the 2 different omics methods—transcriptome analysis allows sensitive detection of molecular perturbations with high coverage of the expressed genome, whereas proteome analysis detects biological players at the effector level.

The salient findings of our open omics approach in omental arterioles exposed to high concentrations of GDP are the upregulation of genes and proteins involved in cell death and apoptosis and deactivation of cell viability and survival, cytoskeleton and junction organization, and immune response biofunctions. These transcriptional perturbations were evident in comparison to both patients before start of dialysis and those on low-GDP PD. Exposure to low-GDP fluids was associated with only minor transcriptional changes in omental arterioles compared to the pre-PD status.

The GDP-related alterations observed in omental arterioles were quantitatively reproduced in parietal peritoneal arterioles, which were also exposed to direct effects of PD fluids, that is, increased glucose concentrations. More lumen narrowing and endothelial cell loss were observed with dialytic GDP exposure. The external circumference was not statistically different in both groups, while the internal circumference was reduced in patients exposed to GDP, that is, the lumen smaller with the intima thickness being significantly higher in high-GDP treated patients. All tissue samples were taken during stable cardiocirculatory conditions under general anesthesia; some impact of the vascular tone on these findings, however, cannot entirely be excluded.

The dialytic glucose load was not statistically different with high- versus low-GDP fluid usage, dialytic GDP load, however, was 4- to 12-fold higher. GDP are not locally retained or metabolized to a major extent[34] but rapidly absorbed, bind nonenzymatically to proteins and lipids, and form AGE. GDP are potent glycating agents; for instance, methylglyoxal is up to 50 000× more reactive than glucose.[35] Circulating AGE concentrations are 20% higher with high-GDP fluid usage.[4,5] In the arterioles studied here, AGE abundance was 2- to 3-fold increased.

In vitro, GDP induces apoptosis of mesothelial cells in the presence of inflammatory cytokines.[36] Administration of methylglyoxal in rats leads to vascular AGE deposition, endothelial cell loss, and lumen narrowing.[37] AGE induce extracellular protein crosslinking, reduce vascular elasticity, bind to RAGE, and activate proinflammatory NF (nuclear factor)-κB and apoptosis.[38,39] We now demonstrate in humans that GDP activate apoptotic pathways in omental and parietal arteriolar endothelial cells, with downregulation of lamin-A/C and upregulation of caspase-3. Downregulation of lamin-A/C was evident on transcriptome and proteome level, in parietal arteriolar immunohistochemical quantification, and upon 3,4-DGE exposure in human umbilical arterial endothelial cells and human umbilical vein endothelial cells in vitro. Lamin-A/C stabilize the cell nucleus, are targeted by caspases in the apoptotic process,[40] and are essentially involved in premature aging.[41]

Another mechanism of vasculopathy disclosed by the omics analyses of arterioles relates to the disorganization of the cytoskeleton and cell-cell junctions. ZO-1, an intracellular scaffold protein bridging tight junction claudins to the actin cytoskeleton,[42,43] was not statistically different in abundance in the arterioles with low- and high-GDP exposure. Since junction function depends on spatial molecule distribution, we for the first time applied single-molecule localization microscopy in tissue and demonstrate disruption of the spatial clustering of ZO-1 in the endothelial membrane regions by GDP; the randomness of ZO-1 distribution in the surrounding areas increased. The GDP-related endothelial ZO-1 disruption was reconfirmed in endothelial cells in vitro and resulted in increased paracellular ionic and dextran permeability, that is, disruption of the arterial endothelial cell barrier integrity. The sealing junction CLDN1 was not affected in abundance by GDP but was inversely related with the degree of arteriolar lumen narrowing, again suggesting sealing junction dysfunction as demonstrated for ZO-1.

Myo-1B is an actin depolymerase regulating actin dynamics in vivo nearby cellular membranes[44] and coordinating receptor signaling by arranging the cytoskeleton.[45] We demonstrate Myo-1B upregulation with GDP exposure in the cross-omics analysis in omental arterioles and in parietal arterioles. Altogether, our stepwise approach demonstrates disruption of the endothelial barrier integrity by GDP on several levels as an early event in the multifactorial, gradually progressive development of vasculopathy.[22]

Next to the arteriolar effects of GDP, our studies provide detailed information regarding the effect of GDP on the parietal peritoneum. As previously reported by our group, exposure to low-GDP PD fluids induced VEGF-A and angiogenesis and marked inflammatory cell infiltration.[46] We now demonstrate that exposure to PD fluids with high-GDP content mitigated peritoneal angiogenesis and infiltration of the tissue by

blood leukocytes, macrophages, and mast cells; tryptase release was reduced. Peritoneal VEGF-A, IL-6, IL-17, and IL-33 signaling were substantially reduced. Thus, the peritoneal findings mirror the deactivation of cellular and humoral inflammatory cascades in the omental arterioles exerted by GDP. This observation is supported by experimental studies. Methylglyoxal promotes degradation of hypoxia-inducible factor-1α and inhibits angiogenesis via VEGF.[47] Glyoxylase-1 overexpression in mice reduces tissue methylglyoxal concentrations and scar size after coronary artery ligation; cardiac vessel density increases.[48] The link between peritoneal IL-17, VEGF induction, and angiogenesis has recently been established[24] and is supported here by the correlation of peritoneal IL-17 with VEGF abundance and microvessel density. Activated mast cells induce angiogenesis via release of growth factors, interleukins, and matrix metalloproteinases,[49,50] findings which are now underpinned by the correlation of peritoneal VEGF-A abundance with tryptase released from activated mast cells.

The GDP-driven induction of multiple pathways involved in vasculopathy as demonstrated in omental arterioles and the advanced lumen narrowing developing in parietal arterioles concomitantly exposed to high-GDP and glucose concentrations is of great concern in view of the exceedingly high cardiovascular disease risk of patients with advanced CKD.[2,51,52] Small arteries and precapillary arterioles control peripheral resistance and microcirculation; thus, our findings are of clinical relevance and mandate treatment strategies designed to reduce systemic GDP load, such as the application of low-GDP dialysis fluids in patients on PD. Innovative strategies may comprise targeting of endothelial barrier dysfunction, for example, by supplementation of alanyl glutamine[53,54] and interventions improving GDP detoxification[55] or administration of scavengers, such as histidine-containing peptides resistant to degradation by carnosinase-1.[56]

Limitations of this study consisted of the low number of omental tissues available from children on high-GDP PD treatment, fulfilling the rigorous inclusion criteria and tissue quality criteria. The untargeted multiomics discovery analyses identified distinct arteriolar pathways and were followed by enrichment analysis of biological processes applying FDR and Benjamini-Hochberg correction. These processes were subsequently validated in different tissues with different methodological approaches and targets. Still, false associations cannot entirely be excluded. The quantitative validation of the transcriptome and proteome could not be obtained in the same tissues with reasonable power, but in arterioles simultaneously exposed to high glucose concentrations. Since the dialytic glucose load was not statistically different in patients treated with low- and high-GDP fluids, the findings could not only be validated but extended to a model with similarities to patients with diabetes and with significant endothelial cell loss and advanced lumen narrowing. Within the purpose of this study, we analyzed the most striking arteriolar omics findings. The comprehensive arteriolar gene and protein data sets represent a unique source of data, suggesting several other pathomechanisms of interest, for example, suppression of radical scavenging, and lipid and carbohydrate metabolism perturbation, which deserve extended studies.

In conclusion, our comprehensive studies demonstrate major GDP-induced pathomechanisms of arteriolar remodeling in children on chronic PD. These findings question the use of high-GDP PD fluids and should redirect the focus of research and therapeutic interventions to targeting GDP overload in CKD, improvement of GDP clearance, and improving vascular endothelial integrity.

ARTICLE INFORMATION

Received April 12, 2021; revision received June 22, 2021; accepted July 6, 2021.

Affiliations

Center for Pediatric and Adolescent Medicine (M.B., C.Z., B.S., I.D., E.L., I.M., F.S., S.G.Z., C.P.S.), Kirchhoff Institute for Physics (D.R., G.H.), Institute of Pathology (C.E.), and Division of Pediatric Surgery, Department of General, Visceral and Transplantation Surgery (P.R.), University of Heidelberg, Heidelberg, Germany. Christian Doppler Laboratory for Molecular Stress Research in Peritoneal Dialysis, Division of Pediatric Nephrology and Gastroenterology, Department of Pediatrics and Adolescent Medicine, Comprehensive Center for Pediatrics, Medical University of Vienna, Vienna, Austria (R.H., M.U., A.W., K.K.). ELKH-SE, Pediatrics and Nephrology Research Group, Budapest, Hungary (E.L.). 1st Department of Pediatrics, Semmelweis University, Budapest, Hungary (E.L., P.S.). Division of Nephrology, Heidelberg University Hospital, Heidelberg, Germany (A.U.). Children's Mercy Kansas City, Kansas City, MO (B.A.W.). Department of Physiology, Faculty of Medicine, University of Thessaly, Larissa, Greece (S.G.Z.).

Acknowledgments

We thank the NCT (National Center for Tumor Diseases) and the Institute of Pathology for technical support. We gratefully acknowledge colleagues (listed in the Appendix in the Data Supplement) who contributed over many years to the International Pediatric Peritoneal Biobank. We thank Dr Felix Bestvater, German Cancer Research Center (DKFZ), Heidelberg, for the continuous accessibility to the localization microscope and for his technical support, and Professor Michael Hausmann for his expertise in localization microscopy studies.

Sources of Funding

This work is part of the IMPROVE-PD (Identification and Management of Patients at Risk Outcome and Vascular Events in Peritoneal Dialysis - but please also mention the abbreviation, as this is a known ITN funded by European Union) project that has received funding from the European Union's Horizon 2020 Research and Innovation Programme under the Marie Sklodowska-Curie grant agreement number 812699. M. Bartosova is funded by the Deutsche Forschungsgemeinschaft (DFG, German Research Foundation)—Projektnummer 419826430. The study was supported by SFB1118 (Projektnummer 236360313). C.P. Schmitt has obtained funding from European Nephrology and Dialysis Institute (ENDI). The financial support of the Austrian Federal Ministry of Science, Research and Economy and the National Foundation for Research, Technology, and Development is gratefully acknowledged (R. Herzog, M. Unterwurzacher, A. Wagner, K. Kratochwill). E. Levai was supported by the ÚNKP-18-2 New National Excellence Program of the Ministry of Human Capacities, Hungary, and Jellinek-Harry Scholarship. S.G. Zarogiannis acknowledges the Alexander von Humboldt Stiftung/Foundation for an Experienced Researcher Fellowship (2019–2021) and the International Peritoneal Dialysis Society (ISPD) for an International Cooperation Research Grant (2019–2021).

Disclosures

R. Herzog and K. Kratochwill are consultants of Zytoprotec GmbH, a spin-off of the Medical University Vienna that holds the patent "Carbohydrate-based perito-

neal dialysis fluid comprising glutamine residue" (International Publication Number: WO 2008/106702 A1). The other authors report no conflicts.

Supplemental Materials

Expanded Materials and Methods
Data Supplement Figures I and II
Data Supplement Tables I–VII
Data Supplement Excel File I–III
References 59–62
Appendix

REFERENCES

1. GBD 2017 Causes of Death Collaborators. Global, regional, and national age-sex-specific mortality for 282 causes of death in 195 countries and territories, 1980-2017: a systematic analysis for the Global Burden of Disease Study 2017. *Lancet (London, England).* 2018;392:1736–1788. doi: 10.1016/S0140-6736(18)32203-7
2. de Jager DJ, Grootendorst DC, Jager KJ, van Dijk PC, Tomas LM, Ansell D, Collart F, Finne P, Heaf JG, De Meester J, et al. Cardiovascular and noncardiovascular mortality among patients starting dialysis. *JAMA.* 2009;302:1782–1789. doi: 10.1001/jama.2009.1488
3. Schmitt CP, Haraldsson B, Doetschmann R, Zimmering M, Greiner C, Böswald M, Klaus G, Passlick-Deetjen J, Schaefer F. Effects of pH-neutral, bicarbonate-buffered dialysis fluid on peritoneal transport kinetics in children. *Kidney Int.* 2002;61:1527–1536. doi: 10.1046/j.1523-1755.2002.00255.x
4. Zeier M, Schwenger V, Deppisch R, Haug U, Weigel K, Bahner U, Wanner C, Schneider H, Henle T, Ritz E. Glucose degradation products in PD fluids: do they disappear from the peritoneal cavity and enter the systemic circulation? *Kidney Int.* 2003;63:298–305. doi: 10.1046/j.1523-1755.2003.00705.x
5. Schmitt CP, von Heyl D, Rieger S, Arbeiter K, Bonzel KE, Fischbach M, Misselwitz J, Pieper AK, Schaefer F; Mid European Pediatric Peritoneal Dialysis Study Group (MEPPS). Reduced systemic advanced glycation end products in children receiving peritoneal dialysis with low glucose degradation product content. *Nephrol Dial Transplant.* 2007;22:2038–2044. doi: 10.1093/ndt/gfm148
6. Himmele R, Jensen L, Fenn D, Ho CH, Sawin DA, Diaz-Buxo JA. A new neutral-pH low-GDP peritoneal dialysis fluid. *Perit Dial Int.* 2012;32:444–452. doi: 10.3747/pdi.2011.00072
7. Frischmann M, Spitzer J, Fünfrocken M, Mittelmaier S, Deckert M, Fichert T, Pischetsrieder M. Development and validation of an HPLC method to quantify 3,4-dideoxyglucosone-3-ene in peritoneal dialysis fluids. *Biomed Chromatogr.* 2009;23:843–851. doi: 10.1002/bmc.1194
8. Mittelmaier S, Fünfrocken M, Fenn D, Berlich R, Pischetsrieder M. Quantification of the six major α-dicarbonyl contaminants in peritoneal dialysis fluids by UHPLC/DAD/MSMS. *Anal Bioanal Chem.* 2011;401:1183–1193. doi: 10.1007/s00216-011-5195-9
9. Blake PG. Is the peritoneal dialysis biocompatibility hypothesis dead? *Kidney Int.* 2018;94:246–248. doi: 10.1016/j.kint.2018.04.014
10. Christensen KL, Mulvany MJ. Location of resistance arteries. *J Vasc Res.* 2001;38:1–12. doi: 10.1159/000051024
11. Neu AM, Sander A, Borzych-Duzalka D, Watson AR, Vallés PG, Ha IS, Patel H, Askenazi D, Balasz-Chmielewska I, Lauronen J, et al; IPPN investigators. Comorbidities in chronic pediatric peritoneal dialysis patients: a report of the International Pediatric Peritoneal Dialysis Network. *Perit Dial Int.* 2012;32:410–418. doi: 10.3747/pdi.2012.00124
12. Herzog R, Boehm M, Unterwurzacher M, Wagner A, Parapatics K, Májek P, Mueller AC, Lichtenauer A, Bennett KL, Alper SL, et al. Effects of Alanyl-glutamine treatment on the peritoneal dialysis effluent proteome reveal pathomechanism-associated molecular signatures. *Mol Cell Proteomics.* 2018;17:516–532. doi: 10.1074/mcp.RA117.000186
13. Hausmann M, Ilić N, Pilarczyk G, Lee JH, Logeswaran A, Borroni AP, Krufczik M, Theda F, Waltrich N, Bestvater F, et al. Challenges for super-resolution localization microscopy and biomolecular fluorescent nano-probing in cancer research. *Int J Mol Sci.* 2017;18:E2066. doi: 10.3390/ijms18102066
14. Lemmer P, Gunkel M, Baddeley D, Kaufmann R, Urich A, Weiland Y, Reymann J, Müller P, Hausmann M, Cremer C. SPDM: light microscopy with single-molecule resolution at the nanoscale. *Appl Phys B.* 2008;93:1.
15. Braun N, Alscher DM, Fritz P, Edenhofer I, Kimmel M, Gaspert A, Reimold F, Bode-Lesniewska B, Ziegler U, Biegger D, et al. Podoplanin-positive cells are a hallmark of encapsulating peritoneal sclerosis. *Nephrol Dial Transplant.* 2011;26:1033–1041. doi: 10.1093/ndt/gfq488
16. Serban AI, Stanca L, Geicu OI, Munteanu MC, Dinischiotu A. RAGE and TGF-β1 cross-talk regulate extracellular matrix turnover and cytokine synthesis in AGEs exposed fibroblast cells. *PLoS One.* 2016;11:e0152376. doi: 10.1371/journal.pone.0152376
17. Bartosova M, Schaefer B, Bermejo JL, Tarantino S, Lasitschka F, Macher-Goeppinger S, Sinn P, Warady BA, Zaloszyc A, Parapatics K, et al. Complement activation in peritoneal dialysis-induced arteriolopathy. *J Am Soc Nephrol.* 2018;29:268–282. doi: 10.1681/ASN.2017040436
18. Zeng L, Dang TA, Schunkert H. Genetics links between transforming growth factor β pathway and coronary disease. *Atherosclerosis.* 2016;253:237–246. doi: 10.1016/j.atherosclerosis.2016.08.029
19. Utech M, Mennigen R, Bruewer M. Endocytosis and recycling of tight junction proteins in inflammation. *J Biomed Biotechnol.* 2010;2010:484987. doi: 10.1155/2010/484987
20. Bojarski C, Weiske J, Schöneberg T, Schröder W, Mankertz J, Schulzke JD, Florian P, Fromm M, Tauber R, Huber O. The specific fates of tight junction proteins in apoptotic epithelial cells. *J Cell Sci.* 2004;117:2097–2107. doi: 10.1242/jcs.01071
21. Flavahan NA. In Development-A New Paradigm for Understanding Vascular Disease. *J Cardiovasc Pharmacol.* 2017;69:248–263. doi: 10.1097/FJC.0000000000000480
22. Chistiakov DA, Orekhov AN, Bobryshev YV. Endothelial Barrier and Its Abnormalities in Cardiovascular Disease. *Front Physiol.* 2015;6:365. doi: 10.3389/fphys.2015.00365
23. Boyd PS, Struve N, Bach M, Eberle JP, Gote M, Schock F, Cremer C, Kriegs M, Hausmann M. Clustered localization of EGFRvIII in glioblastoma cells as detected by high precision localization microscopy. *Nanoscale.* 2016;8:20037–20047. doi: 10.1039/c6nr05880a
24. Witowski J, Kamhieh-Milz J, Kawka E, Catar R, Jörres A. IL-17 in peritoneal dialysis-associated inflammation and angiogenesis: conclusions and perspectives. *Front Physiol.* 2018;9:1694. doi: 10.3389/fphys.2018.01694
25. Altara R, Ghali R, Mallat Z, Cataliotti A, Booz GW, Zouein FA. Conflicting vascular and metabolic impact of the IL-33/sST2 axis. *Cardiovasc Res.* 2018;114:1578–1594. doi: 10.1093/cvr/cvy166
26. López-Cabrera M. Mesenchymal conversion of mesothelial cells is a key event in the pathophysiology of the peritoneum during peritoneal dialysis. *Adv Med.* 2014;2014:473134. doi: 10.1155/2014/473134
27. Nigro C, Leone A, Fiory F, Prevenzano I, Nicolò A, Mirra P, Beguinot F, Miele C. Dicarbonyl stress at the crossroads of healthy and unhealthy aging. *Cells.* 2019;8:E749. doi: 10.3390/cells8070749
28. Nandi A, Yan LJ, Jana CK, Das N. Role of catalase in oxidative stress- and age-associated degenerative diseases. *Oxid Med Cell Longev.* 2019;2019:9613090. doi: 10.1155/2019/9613090
29. Schalkwijk CG, Stehouwer CDA. Methylglyoxal, a highly reactive dicarbonyl compound, in diabetes, its vascular complications, and other age-related diseases. *Physiol Rev.* 2020;100:407–461. doi: 10.1152/physrev.00001.2019
30. Koutroumpakis E, Jozwik B, Aguilar D, Taegtmeyer H. Strategies of unloading the failing heart from metabolic stress. *Am J Med.* 2020;133:290–296. doi: 10.1016/j.amjmed.2019.08.035
31. Busch M, Franke S, Müller A, Wolf M, Gerth J, Ott U, Niwa T, Stein G. Potential cardiovascular risk factors in chronic kidney disease: AGEs, total homocysteine and metabolites, and the C-reactive protein. *Kidney Int.* 2004;66:338–347. doi: 10.1111/j.1523-1755.2004.00736.x
32. Htay H, Johnson DW, Wiggins KJ, Badve SV, Craig JC, Strippoli GF, Cho Y. Biocompatible dialysis fluids for peritoneal dialysis. *Cochrane Database Syst Rev.* 2018;10:CD007554. doi: 10.1002/14651858.CD007554.pub3
33. Flessner MF, Fenstermacher JD, Dedrick RL, Blasberg RG. A distributed model of peritoneal-plasma transport: tissue concentration gradients. *Am J Physiol.* 1985;248:F425–F435. doi: 10.1152/ajprenal.1985.248.3.F425
34. Schaefer B, Bartosova M, Macher-Goeppinger S, Sallay P, Vörös P, Ranchin B, Vondrak K, Ariceta G, Zaloszyc A, Bayazit AK, et al. Neutral pH and low-glucose degradation product dialysis fluids induce major early alterations of the peritoneal membrane in children on peritoneal dialysis. *Kidney Int.* 2018;94:419–429. doi: 10.1016/j.kint.2018.02.022
35. Tauer A, Bender TO, Fleischmann EH, Niwa T, Jörres A, Pischetsrieder M. Fate of the glucose degradation products 3-deoxyglucosone and glyoxal during peritoneal dialysis. *Mol Nutr Food Res.* 2005;49:710–715. doi: 10.1002/mnfr.200400111
36. Thornalley PJ. Dicarbonyl intermediates in the maillard reaction. *Ann N Y Acad Sci.* 2005;1043:111–117. doi: 10.1196/annals.1333.014
37. Santamaría B, Ucero AC, Benito-Martin A, Vicent MJ, Orzáez M, Celdrán A, Selgas R, Ruíz-Ortega M, Ortiz A. Biocompatibility reduces inflammation-induced apoptosis in mesothelial cells exposed to peritoneal dialysis fluid. *Blood Purif.* 2015;39:200–209. doi: 10.1159/000374103

38. Berlanga J, Cibrian D, Guillén I, Freyre F, Alba JS, Lopez-Saura P, Merino N, Aldama A, Quintela AM, Triana ME, et al. Methylglyoxal administration induces diabetes-like microvascular changes and perturbs the healing process of cutaneous wounds. *Clin Sci (Lond).* 2005;109:83–95. doi: 10.1042/CS20050026
39. Fishman SL, Sonmez H, Basman C, Singh V, Poretsky L. The role of advanced glycation end-products in the development of coronary artery disease in patients with and without diabetes mellitus: a review. *Mol Med.* 2018;24:59. doi: 10.1186/s10020-018-0060-3
40. Kosmopoulos M, Drekolias D, Zavras PD, Piperi C, Papavassiliou AG. Impact of advanced glycation end products (AGEs) signaling in coronary artery disease. *Biochim Biophys Acta Mol Basis Dis.* 2019;1865:611–619. doi: 10.1016/j.bbadis.2019.01.006
41. Lindenboim L, Zohar H, Worman HJ, Stein R. The nuclear envelope: target and mediator of the apoptotic process. *Cell Death Discov.* 2020;6:29. doi: 10.1038/s41420-020-0256-5
42. Martins F, Sousa J, Pereira CD, da Cruz E Silva OAB, Rebelo S. Nuclear envelope dysfunction and its contribution to the aging process. *Aging Cell.* 2020;19:e13143. doi: 10.1111/acel.13143
43. Van Itallie CM, Tietgens AJ, Anderson JM. Visualizing the dynamic coupling of claudin strands to the actin cytoskeleton through ZO-1. *Mol Biol Cell.* 2017;28:524–534. doi: 10.1091/mbc.E16-10-0698
44. Rodgers LS, Beam MT, Anderson JM, Fanning AS. Epithelial barrier assembly requires coordinated activity of multiple domains of the tight junction protein ZO-1. *J Cell Sci.* 2013;126:1565–1575. doi: 10.1242/jcs.113399
45. Pernier J, Kusters R, Bousquet H, Lagny T, Morchain A, Joanny JF, Bassereau P, Coudrier E. Myosin 1b is an actin depolymerase. *Nat Commun.* 2019;10:5200. doi: 10.1038/s41467-019-13160-y
46. Freeman SA, Jaumouillé V, Choi K, Hsu BE, Wong HS, Abraham L, Graves ML, Coombs D, Roskelley CD, Das R, et al. Toll-like receptor ligands sensitize B-cell receptor signalling by reducing actin-dependent spatial confinement of the receptor. *Nat Commun.* 2015;6:6168. doi: 10.1038/ncomms7168
47. Williams JD, Craig KJ, Topley N, Von Ruhland C, Fallon M, Newman GR, Mackenzie RK, Williams GT. Morphologic changes in the peritoneal membrane of patients with renal disease. *J Am Soc Nephrol.* 2002;13:470–479. doi: 10.1681/ASN.V132470
48. Thangarajah H, Yao D, Chang EI, Shi Y, Jazayeri L, Vial IN, Galiano RD, Du XL, Grogan R, Galvez MG, et al. The molecular basis for impaired hypoxia-induced VEGF expression in diabetic tissues. *Proc Natl Acad Sci U S A.* 2009;106:13505–13510. doi: 10.1073/pnas.0906670106
49. Blackburn NJR, Vulesevic B, McNeill B, Cimenci CE, Ahmadi A, Gonzalez-Gomez M, Ostojic A, Zhong Z, Brownlee M, Beisswenger PJ, et al. Methylglyoxal-derived advanced glycation end products contribute to negative cardiac remodeling and dysfunction post-myocardial infarction. *Basic Res Cardiol.* 2017;112:57. doi: 10.1007/s00395-017-0646-x
50. Ribatti D, Tamma R, Vacca A. Mast cells and angiogenesis in human plasma cell malignancies. *Int J Mol Sci.* 2019;20:481. doi: 10.3390/ijms20030481
51. Ribatti D, Ranieri G. Tryptase, a novel angiogenic factor stored in mast cell granules. *Exp Cell Res.* 2015;332:157–162. doi: 10.1016/j.yexcr.2014.11.014
52. Johnson DW, Brown FG, Clarke M, Boudville N, Elias TJ, Foo MW, Jones B, Kulkarni H, Langham R, Ranganathan D, et al; balANZ Trial Investigators. The effect of low glucose degradation product, neutral pH versus standard peritoneal dialysis solutions on peritoneal membrane function: the balANZ trial. *Nephrol Dial Transplant.* 2012;27:4445–4453. doi: 10.1093/ndt/gfs314
53. Oh J, Wunsch R, Turzer M, Bahner M, Raggi P, Querfeld U, Mehls O, Schaefer F. Advanced coronary and carotid arteriopathy in young adults with childhood-onset chronic renal failure. *Circulation.* 2002;106:100–105. doi: 10.1161/01.cir.0000020222.63035.c0
54. Saran R, Robinson B, Abbott KC, Agodoa LYC, Bhave N, Bragg-Gresham J, Balkrishnan R, Dietrich X, Eckard A, Eggers PW. US Renal Data System 2017 Annual Data Report: Epidemiology of Kidney Disease in the United States. Chapter 3: Morbidity and mortality in patients with CKD. *Am J Kid Dis.* 2017;69:S67–S92. doi: 10.1053/j.ajkd.2018.01.002
55. Bartosova M, Herzog R, Ridinger D, Levai E, Jenei H, Zhang C, González Mateo GT, Marinovic I, Hackert T, Bestvater F, et al. Alanyl-Glutamine restores tight junction organization after disruption by a conventional peritoneal dialysis fluid. *Biomolecules.* 2020;10:E1178. doi: 10.3390/biom10081178
56. Vychytil A, Herzog R, Probst P, Ribitsch W, Lhotta K, Machold-Fabrizii V, Wiesholzer M, Kaufmann M, Salmhofer H, Windpessl M, et al. A randomized controlled trial of alanyl-glutamine supplementation in peritoneal dialysis fluid to assess impact on biomarkers of peritoneal health. *Kidney Int.* 2018;94:1227–1237. doi: 10.1016/j.kint.2018.08.031
57. Hanssen NMJ, Stehouwer CDA, Schalkwijk CG. Methylglyoxal stress, the glyoxalase system, and diabetic chronic kidney disease. *Curr Opin Nephrol Hypertens.* 2019;28:26–33. doi: 10.1097/MNH.0000000000000465
58. Peters V, Yard B, Schmitt CP. Carnosine and diabetic nephropathy. *Curr Med Chem.* 2020;27:1801–1812. doi: 10.2174/0929867326666190326111851
59. Schaefer B, Bartosova M, Macher-Goeppinger S, Ujszaszi A, Wallwiener M, Nyarangi-Dix J, Sallay P, Burkhardt D, Querfeld U, Pfeifle V, et al. Quantitative histomorphometry of the healthy peritoneum. *Sci Rep.* 2016;6:21344. doi: 10.1038/srep21344
60. Honda K, Hamada C, Nakayama M, Miyazaki M, Sherif AM, Harada T, Hirano H; Peritoneal Biopsy Study Group of the Japanese Society for Peritoneal Dialysis. Impact of uremia, diabetes, and peritoneal dialysis itself on the pathogenesis of peritoneal sclerosis: a quantitative study of peritoneal membrane morphology. *Clin J Am Soc Nephrol.* 2008;3:720–728. doi: 10.2215/CJN.03630807
61. Yáñez-Mó M, Lara-Pezzi E, Selgas R, Ramírez-Huesca M, Do-mínguez-Jiménez C, Jiménez-Heffernan JA, Aguilera A, Sánchez-Tomero JA, Bajo MA, Alvarez V, et al. Peritoneal dialysis and epithelial-to-mesenchymal transition of mesothelial cells. *N Engl J Med.* 2003;348:403–413. doi: 10.1056/NEJMoa020809
62. Schindelin J, Arganda-Carreras I, Frise E, Kaynig V, Longair M, Pietzsch T, Preibisch S, Rueden C, Saalfeld S, Schmid B, et al. Fiji: an open-source platform for biological-image analysis. *Nat Methods.* 2012;9:676–682. doi: 10.1038/nmeth.2019